Journal of Physics: Conference Series **1668** (2020) 012040 doi:10.1088/1742-6596/1668/1/012040

Impact of forbidden electron capture in intermediate-mass stars

Dag F Strömberg[1,2], Gabriel Martínez-Pinedo[1,2], Samuel Jones[3,4], Oliver S Kirsebom[5], Frédéric Nowacki[6]

[1] Institut für Kernphysik, Technische Universität Darmstadt, Germany
[2] GSI Helmholtzzentrum für Schwerionenforschung, Germany
[3] Heidelberger Institut für Theoretische Studien, Germany
[4] X Computational Physics Division, Los Alamos National Laboratory, USA
[5] Department of Physics and Astronomy, Aarhus University, Denmark
[6] Université de Strasbourg, CNRS, IPHC UMR 7178, France

Abstract. Intermediate-mass stars (7–11 $M_\odot$) form degenerate ONe cores following carbon burning. In some cases the cores grow dense enough to trigger electron capture on various nuclei. The double electron capture $^{20}\mathrm{Ne}(e^-,\nu_e)^{20}\mathrm{F}(e^-,\nu_e)^{20}\mathrm{O}$ releases enough heat to trigger runaway oxygen burning. Depending on the conditions at ignition the outcome is either a collapse to a neutron star or a thermonuclear explosion with an ONeFe remnant. We have investigated the impact of two forbidden transitions on the ignition conditions using the MESA stellar evolution code. The $0^+ \rightarrow 2^+$ transition between the ground states of ^{20}Ne and ^{20}F has been measured experimentally and is found to decrease the ignition density while pushing the point of ignition off-centre. We have also studied the $2^+ \rightarrow 4^+$ transition between ^{24}Na and ^{24}Ne through a shell model calculation. Its impact is found to be marginal in our simulations, but it might play a role in the development of convectional instabilities.

1. Introduction

Stars with an initial mass of roughly 7–11 $M_\odot$ fill the intermediate-mass gap between low-mass and massive stars. While it is known that low-mass stars end as carbon-oxygen white dwarfs and massive stars are progenitors to core-collapse supernovae, the fate of stars in the intermediate-mass category is still a matter of debate. [1]

After going through hydrogen, helium and carbon burning such stars enter the Super-AGB phase. In the centre they have a degenerate oxygen-neon (ONe) core consisting mostly of ^{16}O and ^{20}Ne, with minor amount of ^{23}Na, ^{24}Mg and ^{25}Mg. Through thermal pulses mass is added to the core causing it to contract, with the chemical potential of the electrons increasing as $\mu_e \propto \rho^{1/3}$. If the stellar envelope is not expelled first, the core can reach densities where electron capture reactions can occur due to the large μ_e. Most notably we get the exothermic double electron capture

Content from this work may be used under the terms of the Creative Commons Attribution 3.0 licence. Any further distribution of this work must maintain attribution to the author(s) and the title of the work, journal citation and DOI.
Published under licence by IOP Publishing Ltd

Impact of forbidden electron capture in intermediate-mass stars

$^{20}\mathrm{Ne}(e^-,\nu_e)^{20}\mathrm{F}(e^-,\nu_e)^{20}\mathrm{O}$ which raises the temperature to a point where a runaway oxygen burning is triggered.

The outcome depends on the condition at the point of ignition, especially the density. If the central density $\rho_{\mathrm{c}}^{\mathrm{ign}}$ is larger than a critical value $\rho_{\mathrm{c}}^{\mathrm{crit}}$ the result is a collapse to a neutron star. If $\rho_{\mathrm{c}}^{\mathrm{ign}}$ is smaller than $\rho_{\mathrm{c}}^{\mathrm{crit}}$ we instead get a thermonuclear explosion with the remnant being an oxygen-neon-iron (ONeFe) white dwarf. Recent three-dimensional hydrodynamical simulations [2] of the oxygen deflagration indicate that the critical density $\rho_{\mathrm{crit}}^{c} \sim 1 - 2 \times 10^{10}\,\mathrm{g\,cm^{-3}}$.

2. Electron capture processes

To determine $\rho_{\mathrm{ign}}^{\mathrm{c}}$ and thus the outcome of such events we must be able to accurately simulate the evolution leading up to the ignition. This encompasses aspects such as initial composition and the impact of convection, but also the accurate treatment of the relevant electron capture processes. In chronological order capture will occur on ^{23}Na, ^{25}Mg, ^{24}Mg, ^{24}Na and ^{25}Na before the densities required for the final capture on ^{20}Ne are reached.

The effect of the electron capture depends on whether the capturing nucleus has an odd or even mass number. For even nuclei we in general get an exothermic double electron capture (e.g. $^{20}\mathrm{Ne}(e^-,\nu_e)^{20}\mathrm{F}(e^-,\nu_e)^{20}\mathrm{O}$). Capture on odd nuclei on the other hand produce Urca cycles of electron capture and beta decay (e.g. $^{25}\mathrm{Mg} \leftrightarrow {}^{25}\mathrm{Na}$) that cool by releasing large amount of neutrinos. This difference come from odd-even effects which make the energy threshold for the second electron capture (e.g. $^{20}\mathrm{F}(e^-,\nu_e)^{20}\mathrm{O}$) lower than the first ($^{20}\mathrm{Ne}(e^-,\nu_e)^{20}\mathrm{F}$) for even nuclei, but opposite for odd nuclei. In the latter case we can instead get a second set of Urca cycles (e.g. $^{25}\mathrm{Na} \leftrightarrow {}^{25}\mathrm{Ne}$) when μ_e has increased further.

Since the temperature in this phase is comparatively low ($T < 1$ GK) only the most low-lying nuclear states are thermally populated to a significant degree. This means that all relevant electron capture and beta decay rates are determined by a limited number of transitions, most of which are known experimentally. An exception has hitherto been two forbidden transitions that we discuss in this contribution.

3. Impact of $^{20}\mathrm{Ne} \rightarrow {}^{20}\mathrm{F}$ forbidden transition

The $0^+ \rightarrow 2^+$ transition between the ground states of ^{20}Ne and ^{20}F is second forbidden and thus orders of magnitude weaker than the allowed $0^+ \rightarrow 1^+$ transition to the first excited state of ^{20}F. However, as pointed out in [3] the $0^+ \rightarrow 2^+$ transition can still dominate in a critical density regime since its energy threshold is 1 MeV lower than for the $0^+ \rightarrow 1^+$ transition.

This forbidden transition was measured for the first time in a recent experiment in Jyväskylä [4] and found to have an unusual large strength corresponding to $\log(ft) = 10.89(11)$. In [5] we evaluate the impact on the density and geometry

Impact of forbidden electron capture in intermediate-mass stars

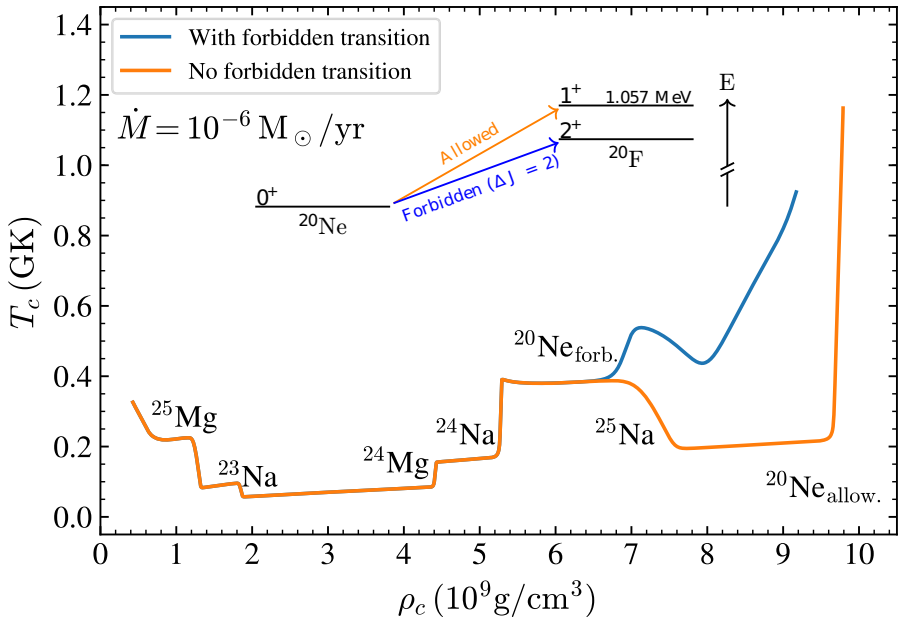

Figure 1. Central temperature as a function of the central density with and without the forbidden transition. The inclusion of the forbidden transition (as illustrated in the energy level diagram) allows capture on ^{20}Ne at earlier densities due to a lower threshold for capture.

of the oxygen ignition. We use the MESA stellar evolution code [6] and simulate contracting degenerate ONe cores following the procedure of [7, 8]: A degenerate core with the composition 50% ^{16}O, 39% ^{20}Ne, 5% ^{23}Na, 5% ^{24}Mg and 1% ^{25}Mg is prepared with a central density of $0.4 \times 10^9\,\mathrm{g\,cm^{-3}}$. Mass is then added at a constant rate $\dot{M} \approx 10^{-6}\ M_\odot/\mathrm{yr}$ to simulate the growth from thermal pulses. We use MESA's ability to calculate weak interaction rates on the fly, which we have extended to support second-forbidden transitions.

In Figure 1 we show the central temperature (T_c) of as a function of the central density (ρ_c) for the growth rate $\dot{M} = 10^{-6}\ M_\odot/\mathrm{yr}$ with and without the forbidden transition included. The two cases diverge at $\rho_c \approx 7.0 \times 10^9\,\mathrm{g\,cm^{-3}}$.

Without the forbidden transition the centre of the core will first cool from the ^{25}Na $\leftrightarrow$ ^{25}Ne Urca cycle and then reach the densities needed for capture on ^{20}Ne via the allowed transition at $\rho_c \approx 9.8 \times 10^9\,\mathrm{g\,cm^{-3}}$. The heating from the $^{20}\mathrm{Ne}(e^-,\nu_e)^{20}\mathrm{F}(e^-,\nu_e)^{20}\mathrm{O}$ double electron capture rapidly raises the temperature until oxygen is ignited at the centre.

When the forbidden transition is included the lower energy threshold means that capture on ^{20}Ne can set in before the ^{25}Na $\leftrightarrow$ ^{25}Ne Urca cycle. Due to the weakness of the forbidden transition the heating is gradual and is temporarily cancelled by the Urca cooling. When ^{25}Na has been exhausted in the centre the heating resumes and finally ignites oxygen at a lower density ($\rho_c \approx 9.2 \times 10^9\,\mathrm{g\,cm^{-3}}$) than before.

Impact of forbidden electron capture in intermediate-mass stars

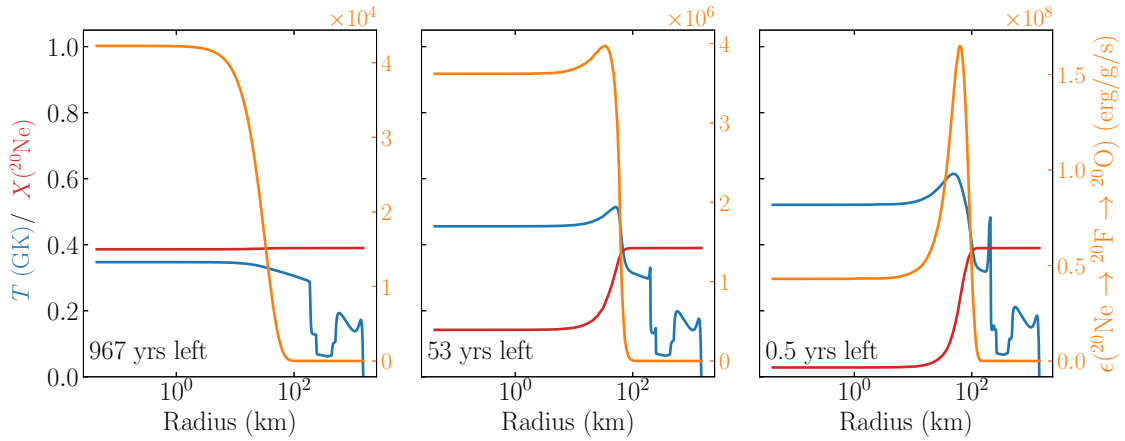

Figure 2. Radial profiles of a simulation with $\dot{M} = 10^{-7}$ $M_\odot$/yr. Note that the horizontal axis is logarithmic. The quantities plotted are the temperature (blue), mass fraction of ^{20}Ne (red) and heating rate from the $^{20}\mathrm{Ne}(e^-,\nu_e)^{20}\mathrm{F}(e^-,\nu_e)^{20}\mathrm{O}$ double electron capture (orange). In the lower left corner the number of years until ignition is listed, with the first frame being at the point when electron capture on ^{20}Ne sets in. The forbidden transition slowly depletes ^{20}Ne in the centre, eventually shifting the point of maximal heating outwards where more ^{20}Ne is left. This results in an off-centre ignition of the oxygen deflagration.

	No $^{20}\mathrm{Ne} \to {}^{20}\mathrm{F}$ forb.		With $^{20}\mathrm{Ne} \to {}^{20}\mathrm{F}$ forb.	
$\dot{M}$	ρ_c^{ign}	R_{ign}	ρ_c^{ign}	R_{ign}
10^{-7}	9.94	0	9.47	58
10^{-6}	9.80	0	9.17	35
10^{-5}	9.59	0	8.65	0

Table 1. Ignition densities and radii with and without the $^{20}\mathrm{Ne} \to {}^{20}\mathrm{F}$ forbidden transition. $\dot{M}$ is in $M_\odot$/yr, ρ_c^{ign} is in $10^9\,\mathrm{g\,cm^{-3}}$ and R_{ign} is in km.

In addition to the change in the ignition density the forbidden transition also alters the ignition geometry. This process is illustrated in Figure 2 for the case $\dot{M} = 10^{-7}$ $M_\odot$/yr. In the $\sim$ 1000 years from the onset of electron capture the forbidden transition has time to convert a substantial amount of ^{20}Ne in the centre to ^{20}O. This gradually shifts the point of maximal heating outwards, leading to an off-centre temperature peak and subsequent ignition 35 km from the centre.

The impact of the forbidden transition for the three growth rates are summarised in Table 1. Note that for slower growth rates the ignition occurs further off-centre, since forbidden transitions gets more time to work. In [5] 3D hydrodynamical simulations corresponding to these conditions are presented. Although all cases in Table 1 give thermonuclear explosions the forbidden transition has an appreciable impact: The lower ignition density results in a more massive ONeFe white dwarf, and the off-centre ignition leads to a higher fraction of iron-group nuclei in the remnant.

4. Preliminary results on ^{24}Na $\rightarrow$ ^{24}Ne forbidden transition

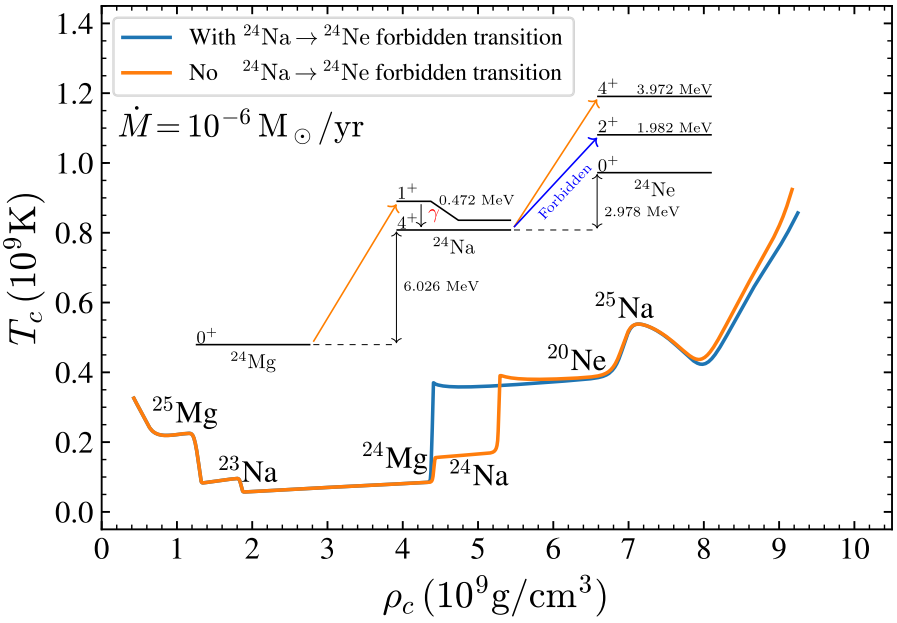

Figure 3. Central temperature as a function fo the central density with and without the ^{24}Na $\rightarrow$ ^{24}Ne forbidden transition. The forbidden transition between the ground states of ^{20}Ne and ^{20}F are included in both cases.

As mentioned in [8], there is an additional second forbidden transition between the 4^+ ground state of ^{24}Na and the 2^+ excited state of ^{24}Ne. We calculated this transition with the `ANTOINE` [9, 10] shell model code and the USDB interaction [11], and using the formalism of Behrens and Bühring [12]. The impact on the central evolution is illustrated in Figure 3. When only allowed transitions are included in the $^{24}\mathrm{Mg}(e^-,\nu_e)^{24}\mathrm{Na}(e^-,\nu_e)^{24}\mathrm{Ne}$ chain a double electron capture does not occur. Instead we get two separated electron capture reactions $^{24}\mathrm{Mg}(e^-,\nu_e)^{24}\mathrm{Na}$ and $^{24}\mathrm{Na}(e^-,\nu_e)^{24}\mathrm{Ne}$, both contributing to an increase in temperature.

The reason for this separation is that the spin-parity of the ^{24}Na ground state is 4^+, whereas the ground states of ^{24}Mg and ^{24}Ne have 0^+. This means that transitions between the ground states are highly forbidden, and that allowed transitions go to excited states only. Whereas the energy threshold for the first ground state to ground state transition is larger than for the second (just as for $^{20}\mathrm{Ne}(e^-,\nu_e)^{20}\mathrm{F}(e^-,\nu_e)^{20}\mathrm{O}$) the opposite is true for the allowed transitions. As a consequence of this the two electron capture processes occur separately, with the heating coming from the deexcitation of the excited states. When including the forbidden transition the threshold for the second step is reduced so that we do get a double electron capture.

The effect on the ignition conditions when including the forbidden transition between ^{24}Na and ^{24}Ne is listed in Table 2. The ignition density and radii both increase,

Impact of forbidden electron capture in intermediate-mass stars

	No ^{24}Na $\rightarrow$ ^{24}Ne forb.		With ^{24}Na $\rightarrow$ ^{24}Ne forb.	
$\dot{M}$	$\rho_c^{\rm ign}$	$R_{\rm ign}$	$\rho_c^{\rm ign}$	$R_{\rm ign}$
10^{-7}	9.47	58	9.55	62
10^{-6}	9.17	35	9.24	42
10^{-5}	8.65	0	8.67	0

Table 2. Ignition densities and radii with and without the ^{24}Na $\rightarrow$ ^{24}Ne forbidden transition. The forbidden transition between the ground states of ^{20}Ne and ^{20}F are included in both cases. $\dot{M}$ is in $M_\odot$/yr, $\rho_c^{\rm ign}$ is in $10^9\,{\rm g\,cm^{-3}}$ and $R_{\rm ign}$ is in km.

but the effects are mostly marginal. As mentioned in [8] however, the transition could play a role in the convectional instabilities that arise following the capture on ^{24}Mg. MESA is currently unable to take these instabilities into account.

Acknowledgements

This work is supported the Deutsche Forschungsgemeinschaft (DFG, German Research Foundation) - Projektnummer 279384907 - SFB 1245 "Nuclei: From Fundamental Interactions to Structure and Stars"; and the ChETEC COST action (CA16117), funded by COST (European Cooperation in Science and Technology).

References

[1] Doherty C L, Gil-Pons P, Siess L and Lattanzio J C 2017 *Publ. Astron. Soc. Aust. 34*, **e056**
[2] Jones S *et al* 2016 *Astron. Astrophys. 593* **A72**
[3] Martínez-Pinedo G, Lam Y H, Langanke K, Zegers R G T and Sullivan C 2014 *Phys. Rev. C* **89** 045806
[4] Kirsebom O S, Hukkanen M, Kankainen A , Trzaska W H, Strömberg D F, Martínez-Pinedo G *et al* arXiv:1805.08149 [nucl-ex]
[5] Kirsebom O S , Jones S, Strömberg D F, Martínez-Pinedo G, Langanke K, Roepke F K *et al* arXiv:1905.09407 [astro-ph.SR]
[6] Paxton B *et al* 2018 *Astrophys. J. Suppl. Ser.* **234** 34
[7] Schwab J, Quataert E and Bildsten L 2015 *Mon. Not. R. Astron. Soc.* **453** 1910–1927
[8] Schwab J, Bildsten L and Quataert E 2017 *Mon. Not. R. Astron. Soc.* **472** 3390–34061
[9] Caurier E, Martinez-Pinedo G, Nowacki F, Poves A and Zuker A P 2005 *Rev. Mod. Phys* **77** 427
[10] Caurier E and Nowacki F 1999 *Acta. Phys. Polonica* B **30** 705
[11] Brown B A and Richter W A 2006 *Phys. Rev. C* **74** 034315
[12] Behrens H and Bühring W 1984 *Electron Radial Wave Functions and Nuclear Beta-decay* (Oxford: Clarendon Press)